J Braz. Soc. Mech. Sci. Eng. (2017) 39:267–277
DOI 10.1007/s40430-016-0499-5

TECHNICAL PAPER

Temperature-dependent shear-thinning Herschel–Bulkley fluid flow by taking into account viscous dissipation

Nabila Labsi[1] · Youb Khaled Benkahla[1] · Abdelkader Boutra[1]

Received: 23 September 2015 / Accepted: 5 February 2016 / Published online: 22 February 2016

Abstract The present numerical study deals with the analysis of hydrodynamic and thermal characteristics of a shear-thinning Herschel–Bulkley fluid flow within a pipe of a circular cross section, maintained at a uniform wall temperature. The governing equations of the studied steady problem are solved using a homemade computer code based on the finite volume method. The paper is focused on the consequences of neglecting the temperature dependency of the fluid's consistency and/or the viscous dissipation on both pressure drop and heat transfer. The results show, indeed, that neglecting the temperature dependency of the fluid's viscosity leads to significantly undervalue these parameters, especially when viscous dissipation is also missed. Abacuses depicting the friction factor of Fanning and the Nusselt number variations according to both Brinkman number and dimensionless temperature coefficient are proposed to sum up the study.

Keywords Shear-thinning Herschel–Bulkley fluid · Viscous dissipation · Temperature-dependent consistency · Uniform wall temperature · Finite volume method

List of symbols

a	Temperature coefficient (K^{-1})
a^*	Dimensionless temperature coefficient, $= a\ \Delta T$
Br	Brinkman number, $K_0 V_0^2 / k(T_0 - T_w)$
C_p	Specific heat at constant pressure (J kg^{-1} K^{-1})
D	Pipe diameter (m)
f	Friction factor
fRe	Friction factor of Fanning
h	Heat transfer coefficient (W m^{-2} K^{-1})
HB	Herschel–Bulkley number, $\tau_0 D^n / K_0 V_0^n$
k	Fluid thermal conductivity (W m^{-1} K^{-1})
K	Fluid consistency (Pa s^n)
K_0	Fluid consistency at the reference temperature (Pa s^n)
K^*	Dimensionless fluid consistency, $K(T)/K_0$
L	Pipe length (m)
m	Exponential growth parameter (s)
M	Dimensionless exponential growth parameter in Eq. (6), $= m\ V_0/D$
n	Flow index
Na	Nahme number, $= a K_0 V_0^2 / k$
Nu	Nusselt number, $= \frac{hD}{k} = \frac{-1}{\theta_m} \frac{\partial \theta}{\partial R}\big\vert_{R=0.5}$
Pe	Peclet number, $= Re\ Pr$
Pr	Prandtl number, $= K_0 C_p V_0^{n-1} / kD^{n-1}$
P^*	Dimensionless pressure, $= p^*/\rho\ V_0^2$
p^*	Pressure (Pa)
r	Radial coordinate (m)
r_p	Plug size (m)
r_0^*	Dimensionless plug size according to [19]
r_0'	Dimensionless plug size, $r_p/(D/2) = \tau_0/\tau_w = r_0^*/2$
R	Dimensionless radial coordinate, $= r/D$
Re	Reynolds number, $= \rho V_0^{2-n} D^n / K_0$
T	Temperature (K)
T_0	Inlet temperature (K)
T_m	Bulk temperature (K)
T_w	Wall temperature (K)
U	Dimensionless x-component velocity, $= V_x/V_0$

Technical Editor: Roney Leon Thompson.

✉ Nabila Labsi
nabilalabsi@yahoo.fr; nlabsi@usthb.dz

[1] Laboratoire des Phénomènes de Transfert, Equipe Rhéologie et Simulation Numérique des Ecoulements, Faculté de Génie Mécanique et de Génie des Procédés, Université des Sciences et de la Technologie Houari Boumediene, B.P. 32, El-Alia Bab-Ezzouar, 16111 Algiers, Algeria

V Dimensionless r-component velocity, $= V_r/V_0$
V_0 Mean velocity (m s^{-1})
V_x x-Component velocity (m s^{-1})
V_r r-Component velocity (m s^{-1})
x Axial coordinate (m)
X Dimensionless axial coordinate, $= x/D$

Greek letters

$\dot{\gamma}$ Rate of strain (s^{-1})
$\dot{\gamma}^*$ Dimensionless rate of strain
ΔT Temperature difference, $= T_w - T_0$ (K)
Δp Pressure drop (Pa)
η Effective viscosity of the Herschel–Bulkleyfluid (Pa s^n)
η_{eff} Dimensionless effective viscosity, $= \eta/K_0$
θ Dimensionless temperature, $= (T - T_w)/(T_0 - T_w)$
θ_m Dimensionless mean temperature, $(T_m - T_w)/(T_0 - T_w)$
ρ Density of the fluid (kg m^{-3})
τ Shear stress (Pa)
τ_0 Yield stress (Pa)
τ_w Wall shear stress (Pa)

Subscripts

asy Asymptotic
av Average
c Centreline
x Local

1 Introduction

Viscoplastic fluids are encountered in both nature and many industrial applications, such as lava, crude oil, mayonnaise, ketchup and concrete. They are characterized by a yield stress from which the fluid starts moving. The Herschel–Bulkley model describes the rheological behaviour of a wide range of this kind of non-Newtonian fluids.

Since several industrial applications deal with viscoplastic fluids flow such as the cosmetic, food, petroleum, paint and pharmaceutical industries, researches have been undertaken to understand the flow behaviour of such fluids [1–8]. In these studies viscous dissipation is either neglected or taken into account and the fluid is of constant rheological properties. Actually, the latter varies according to the temperature, what adds a further complexity to the momentum and energy balance equations. Therefore, analytical and numerical techniques are often needed to obtain solutions. The literature reveals that the most of studies related to viscoplastic fluids consider the case of constant rheological properties while few of them account for their temperature dependency. Duvaut and Lions [9] studied analytically the velocity and temperature fields of a Bingham fluid, by considering the variation of the plastic viscosity according to the temperature. Vinay et al. [10] examined the waxy crude oil transportation into a pipeline, where the flowing oil was cooled down due to extreme external temperature conditions. The situation was simulated numerically by considering the transient non-isothermal flows of a Bingham fluid for which both plastic viscosity and yield stress were assumed to be function of the temperature. Soares et al. [11] studied the developing flow of Herschel–Bulkley materials inside tubes for constant and temperature-dependent rheological properties using a finite volume method. In the same context, Nouar [12] investigated the combined forced and free convection heat transfer via a Herschel–Bulkley fluid in a horizontal duct heated uniformly with a constant heat flux density. Recently, Peixinho et al. [13] undertook an experimental study on the forced convection heat transfer for a temperature-dependent Carbopol aqueous solution by considering a transitional regime and neglecting viscous dissipation.

It is worth noting that viscous dissipation's effect for viscoplastic fluids with temperature-dependent rheological properties has not yet been deeply investigated, especially for the wall heating case which corresponds to negative values of the Brinkman number. We tried in a previous study [14] to investigate this case by considering a viscoplastic fluid obeying the simple rheological model of Bingham, which is a limit case of the Herschel–Bulkley rheological model. Therefore, the present numerical study is a sequel and an extension to the latter. It concerns the simultaneous developing flow of an incompressible shear-thinning Herschel–Bulkley fluid inside a circular pipe maintained at a uniform temperature. This kind of viscoplastic fluids is largely encountered in both nature and industries. Thus, to approach real applications, both viscous dissipation and viscosity's temperature dependency are considered. The effects of these parameters on hydrodynamic and thermal characteristics of the flow are then numerically investigated by means of a computer code based on the finite volume method and on the line by line resolver.

2 Mathematical formulation and numerical resolution

The forced convection heat transfer flow of a fluid of constant physical properties (ρ, C_p and k) within a circular pipe of length L and diameter D is governed by the following dimensionless conservation equations, i.e. mass, momentum and energy equations:

$$\frac{1}{R}\frac{\partial(RV)}{\partial R} + \frac{\partial U}{\partial X} = 0 \tag{1}$$

$$\frac{1}{R}\frac{\partial(RVV)}{\partial R}+\frac{\partial(UV)}{\partial X}=-\frac{\partial P^*}{\partial R}+\frac{1}{Re}\left[\frac{1}{R}\frac{\partial}{\partial R}\left(\eta_{\text{eff}}R\frac{\partial V}{\partial R}\right)+\frac{\partial}{\partial X}\left(\eta_{\text{eff}}\frac{\partial V}{\partial X}\right)\right]+\frac{1}{Re}\left[\frac{V}{R}\frac{\partial}{\partial R}(\eta_{\text{eff}})-\eta_{\text{eff}}\frac{V}{R^2}+\frac{\partial}{\partial X}(\eta_{\text{eff}})\frac{\partial U}{\partial R}+R\frac{\partial}{\partial R}(\eta_{\text{eff}})\frac{\partial}{\partial R}\left(\frac{V}{R}\right)\right] \tag{2}$$

$$\frac{1}{R}\frac{\partial(RVU)}{\partial R}+\frac{\partial(UU)}{\partial X}=-\frac{\partial P^*}{\partial X}+\frac{1}{Re}\left[\frac{1}{R}\frac{\partial}{\partial R}\left(\eta_{\text{eff}}R\frac{\partial U}{\partial R}\right)+\frac{\partial}{\partial X}\left(\eta_{\text{eff}}\frac{\partial U}{\partial X}\right)\right]+\frac{1}{Re}\left[\frac{\partial}{\partial R}(\eta_{\text{eff}})\frac{\partial V}{\partial X}+\frac{\partial}{\partial X}(\eta_{\text{eff}})\frac{\partial U}{\partial X}\right] \tag{3}$$

$$\frac{1}{R}\frac{\partial(RV\theta)}{\partial R}+\frac{\partial(U\theta)}{\partial X}=\frac{1}{Pr\,Re}\left[\frac{1}{R}\frac{\partial}{\partial R}\left(R\frac{\partial\theta}{\partial R}\right)+\frac{\partial^2\theta}{\partial X^2}\right]+\frac{Br}{Pr\,Re}\eta_{\text{eff}}\dot{\gamma}^2 \tag{4}$$

where

$$\dot{\gamma}^{*2}=2\left\{\left(\frac{\partial V}{\partial R}\right)^2+\left(\frac{\partial U}{\partial X}\right)^2+\left(\frac{V}{R}\right)^2\right\}+\left(\frac{\partial U}{\partial R}+\frac{\partial V}{\partial X}\right)^2 \tag{5}$$

The fluid used in the present study obeys the general rheological model of Herschel–Bulkley, given by the following law:

$$\begin{cases}\tau=K\dot{\gamma}^n+\tau_0 & \tau\geq\tau_0\\ \dot{\gamma}=0 & \tau<\tau_0\end{cases} \tag{6}$$

To avoid numerical instabilities in the low shear rate region, many authors [3, 15] recommend the use of the following dimensionless constitutive law proposed by Papanastasiou [16], which relates the dimensionless effective viscosity, η_{eff}, to the dimensionless shear rate $\dot{\gamma}^*$:

$$\eta_{\text{eff}}=\dot{\gamma}^{*n-1}+\frac{HB}{\dot{\gamma}^*}\left[1-\exp\left(-M\dot{\gamma}^*\right)\right] \tag{7}$$

$M = mV_0/D$ is the dimensionless exponential growth parameter. Typically, a value of $m = 1000$ s is considered [3, 17]. $HB=\tau_0D^n/K_0V_0^n$ is the Herschel–Bulkley number which represents the ratio of the yield stress to the nominal shear stress.

To complete the system of governing equations, we consider as steady boundary conditions, a uniform axial velocity and temperature at the inlet ($U=\theta=1$, $V=0$), no-slip conditions are applied at the wall along the pipe where a uniform wall temperature is assumed ($U=V=\theta=0$) and finally, at the outlet, we consider: $\left(\frac{\partial U}{\partial X}=\frac{\partial V}{\partial X}=\frac{\partial\theta}{\partial X}=0\right)$.

To analyse the effect of the temperature dependency of the apparent viscosity on hydrodynamic and thermal behaviour of the flow, we keep constant, in this study, the flow index and the yield stress and we consider only a temperature-dependent consistency $K(T)$ described by the following exponential function used by many authors such as Sares et al. [11] and Nouar [12]:

$$K(T)=K_0\exp\left[-a(T-T_0)\right] \tag{8}$$

where K_0 is the fluid's consistency evaluated at the reference temperature T_0 (chosen here as the inlet temperature) and a is the temperature coefficient.

Since the present study deals with dimensionless parameters, we substitute the dimensionless temperature into Eq. (8). Thus, the latter can be written as follows:

$$K^*(\theta)=\exp\left[-a^*(1-\theta)\right] \tag{9}$$

where $a^*=a\Delta T$ depicts the dimensionless temperature coefficient and $K^*(\theta)=K(T)/K(T_0)$ is the dimensionless fluid consistency. The heating and the cooling cases correspond, respectively, to a positive and to a negative value of the coefficient a^* ($a^*>0$ and $a^*<0$) whereas the case of a constant viscosity is obtained for $K^*(\theta)=1$.

Thus, the chosen dimensional analysis, for the case of a pipe maintained at a uniform wall temperature, generates the following dimensionless numbers: the Reynolds number which characterizes the ratio of inertial forces to viscous forces, $Re=\rho V_0^{2-n}D^n/K_0$, the Prandtl number, $Pr=K_0C_pV_0^{n-1}/kD^{n-1}$ which represents the ratio of momentum diffusion to thermal diffusion and the Brinkman number, which measures the importance of the viscous heating to the conductive heat transfer $Br=K_0V_0^2/k(T_0-T_w)$.

The pressure drop and heat transfer within the pipe are evaluated throughout the calculation of the friction factor

and the Nusselt number given, respectively, by the following expressions:

$$f = -\frac{\tau_w}{\frac{1}{2}\rho V_0^2} = \frac{1}{\frac{1}{2}\rho V_0^2}\frac{\Delta p D}{4L} \tag{10}$$

$$Nu = \frac{hD}{k} = \frac{-1}{\theta_m}\frac{\partial\theta}{\partial R}\bigg|_{R=0.5} \tag{11}$$

The obtained set of equations with the corresponding boundary conditions are solved numerically using the finite volume method proposed by Patankar [18]. This widely used method ensures a complete conservation of mass, momentum and energy in the computational domain. Furthermore, it allows the simulation of both actual and ideal conditions. It is based on subdividing the calculation domain in a finite number of control volumes, also called grid cells. The basic principle of this method is to integrate the differential governing equations over each cell (control volume) surrounding the calculating point, called the principal node, within a staggered grid. The scalar variables (pressure and temperature) are located at the centre of each cell while the velocity components are defined at the cell faces. Thus, the differential governing equations are transformed in algebraic equations which are solved by means of the line by line method. The grid adopted in the present paper is non-uniform and consists, after studying the sensitivity of the results to the mesh, of 250 nodes in the X direction and 50 nodes in the R direction. The convergence criterion, which is based on the residual, is set to 10^{-5} for both velocity components and temperature and to 10^{-6} for pressure.

3 Results and discussion

We proceed in this section to the validation of the computer code. This validation highlights also the effect of the Herschel–Bulkley number on hydrodynamic and thermal characteristics of a shear-thinning Herschel–Bulkley fluid's flow, for which the flow index is taken equal to 0.5.

This validation and parametric study will be followed by the analysis of heat and flow properties when taking into account a temperature-dependent consistency, first by neglecting viscous dissipation and then, by taking it into account. The investigations will be carried out for the following values: $Pr = 50$, $Re = 20$ (i.e. $Pe = 1000$) and $HB = 2$.

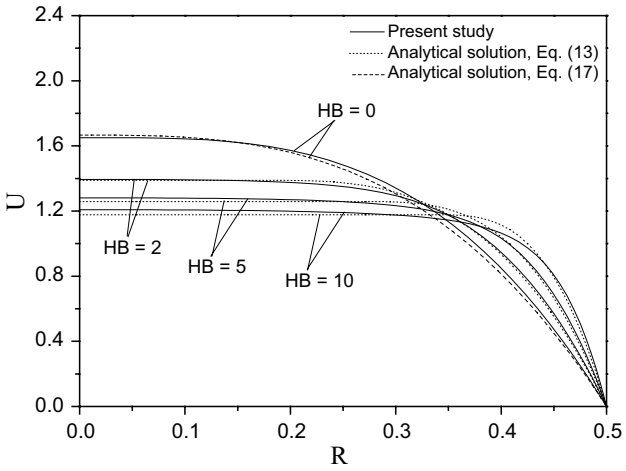

Fig. 1 Fully developed velocity profiles for various values of the Herschel–Bulkley number. $Re = 20$, $Pr = 50$, $Br = 0$

3.1 Validation of the computer code: effect of the Herschel–Bulkley number

Viscoplastic fluids are characterized by a dimensionless number which represents the ratio of the yield stress to the nominal shear stress; for a Herschel–Bulkley fluid, it is called the Herschel–Bulkley number.

Figure 1 shows the fully developed velocity profiles for various values of the Herschel–Bulkley number when neglecting viscous dissipation ($Br = 0$). We note that all the curves, except the one corresponding to $HB = 0$ (shear-thinning power-law fluid), present two regions: a region close to the wall characterized by a parabolic velocity profile (yielded region) and a zone around the centreline which represents a uniform velocity distribution, called "core region" (unyielded region). In the last region, the shear stress is less than the yield stress, the fluid resists consequently to deformations and moves like a rigid solid.

Figure 1 illustrates also a comparison between the numerical results and those obtained from the following analytical solution for the fully developed velocity profile [19], adapted to our dimensionless parameters:

$$U = \begin{cases} \frac{n}{n+1}\left(\frac{HB}{r_0'}\right)^{1/n}\left(\frac{1}{2}-r_0'\right)^{(n+1)/n} & 0 \le R \le r_0' \\ \frac{n}{n+1}\left(\frac{HB}{r_0'}\right)^{1/n}\left[\left(\frac{1}{2}-r_0'\right)^{(n+1)/n} - \left(R-r_0'\right)^{(n+1)/n}\right] & r_0' \le R \le \frac{1}{2} \end{cases} \tag{12}$$

Table 1 Dimensionless plug size for various values of the Herschel–Bulkley number

HB	2	5	10
r_0'	0.221	0.275	0.340

$Pr = 50$, $Re = 20$, $Br = 0$

r_0' is the dimensionless plug size which corresponds, in our dimensionless writing, to: $r_0' = r_0^*/2$. r_0^* is the dimensionless plug size in the paper of [19].

When considering a flow index n equal to 0.5, Eq. (12) becomes:

$$U = \begin{cases} \frac{1}{3}\left(\frac{HB}{r_0'}\right)^2\left(\frac{1}{2} - r_0'\right)^3 & 0 \le R \le r_0' \\ \frac{1}{3}\left(\frac{HB}{r_0'}\right)^2\left[\left(\frac{1}{2} - r_0'\right)^3 - \left(R - r_0'\right)^3\right] & r_0' \le R \le \frac{1}{2} \end{cases} \tag{13}$$

The dimensionless plug size r_0' is calculated from the following equation [19], adapted as well, to our dimensionless parameters:

$$0 = \left(1 - r_0'\right)^{(3n+1)/n} - \frac{(3n+1)}{n}\left(1 - r_0'\right)^{(2n+1)/n} + \frac{(3n+1)(2n+1)}{2n^2}\left(1 - r_0'\right)^{(n+1)/n} - \frac{(3n+1)(2n+1)(n+1)}{2n^3}\left(\frac{2^n r_0'}{HB}\right)^{1/n} \tag{14}$$

For the case $n = 0.5$, Eq. (14) becomes:

$$0 = \left(1 - r_0'\right)^5 - 5\left(1 - r_0'\right)^4 + 10\left(1 - r_0'\right)^3 - 30\left(\frac{2^{0.5} r_0'}{HB}\right)^2 \tag{15}$$

The numerical and analytical solutions are in good agreement since the difference between both results does not exceed 1.75, 2.60 and 3.90 % for, respectively, $HB = 2$, 5 and 10.

On the other hand, for $HB = 0$, the fluid can be described by the power-law model, for which the fully developed velocity profile is given by the following equation [20]:

$$U = \frac{3n+1}{n+1}\left[1 - (2R)^{(n+1)/n}\right] \tag{16}$$

i.e. for $n = 0.5$:

$$U = \frac{5}{3}\left[1 - (2R)^3\right] \tag{17}$$

The comparison between the numerical results and those calculated from Eq. (17) for the case of a shear-thinning fluid shows a good agreement since the difference between both results is about 2.95 %.

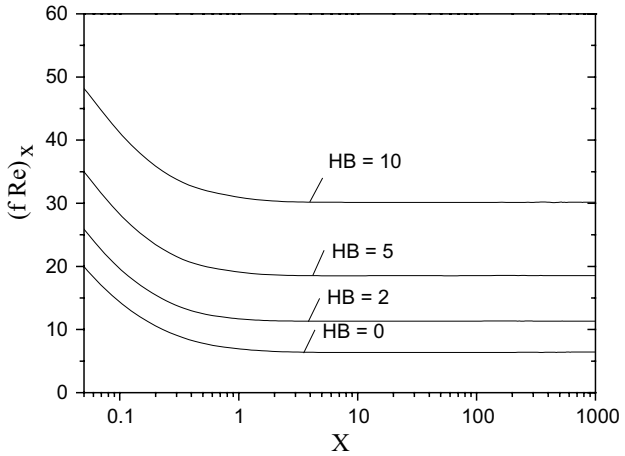

Fig. 2 Axial evolution of the friction factor of Fanning for various values of the Herschel–Bulkley number. $Re = 20$, $Pr = 50$, $Br = 0$

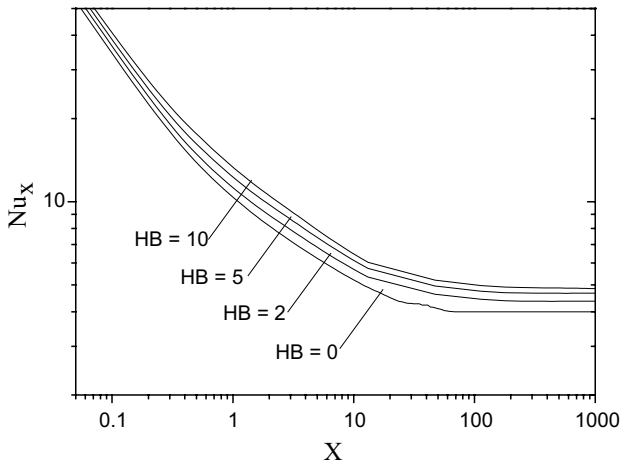

Fig. 3 Axial evolution of local Nusselt number for various values of the Herschel–Bulkley number. $Re = 20$, $Pr = 50$, $Br = 0$

From the calculation of the dimensionless plug size using Eq. (15), by means of an iterative calculation in Excel, we can note from the results gathered in Table 1 that the increase of the Herschel–Bulkley number leads to the increase of the dimensionless plug size, i.e. the extension of the unyielded region.

Regarding the effect of the Herschel–Bulkley number variation on both the friction factor of Fanning ($f\,Re$) and the local Nusselt number, it can be seen from Figs. 2 and 3 that the increase of the Herschel–Bulkley number improves somehow heat transfer at the inlet of the pipe but this effect is not very significant in the fully developed region. However, the friction factor of Fanning is more sensitive to the variation of the Herschel–Bulkley number since its increase leads to the increase of this coefficient and thus, to an important raise of the pressure drop throughout the pipe [Eq. (10)].

Table 2 Asymptotic values of the friction factor of Fanning and the Nusselt number according to the Herschel–Bulkley number

HB	$(f\,Re)_{x\ asy}$		$Nu_{x\ asy}$	
	Present study	Quaresma and Macêdo [21]	Present study	Quaresma and Macêdo [21]
0	6.3400	6.32455	4.0260	3.9494
5	18.4888	18.1880	4.6576	4.6722
10	30.1535	29.3964	4.8880	4.9474

$Re = 20$, $Pr = 50$, $Br = 0$

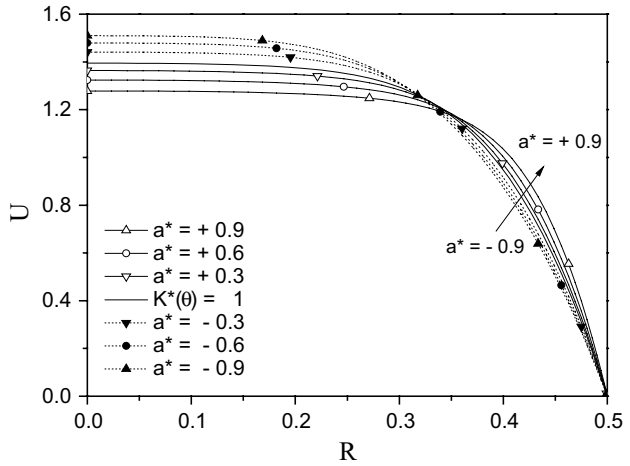

Fig. 4 Fully developed velocity profile for various values of the dimensionless temperature coefficient. $Re = 20$, $Pr = 50$, $HB = 2$, $Br = 0$

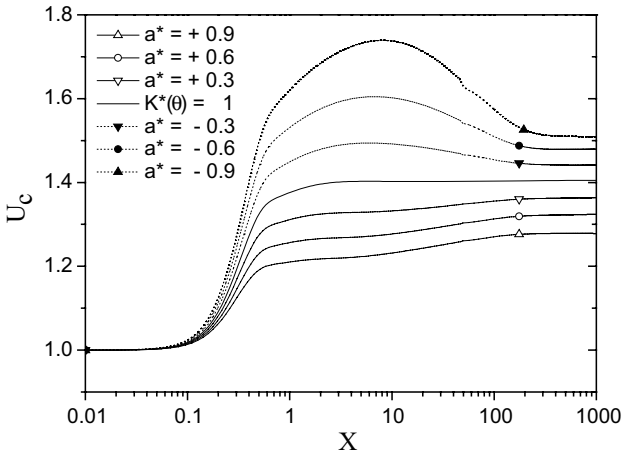

Fig. 5 Axial evolution of the centreline velocity for various values of the dimensionless temperature coefficient. $Re = 20$, $Pr = 50$, $HB = 2$, $Br = 0$

The same behaviour has been observed by Quaresma and Macêdo [21] in their numerical study. According to Table 2, we can see that the asymptotic values of both the friction factor of Fanning and the Nusselt number obtained from our study approach closely those obtained by these authors.

3.2 Temperature-dependent consistency

Viscoplastic fluids are known to be very viscous. Most of the time in practice, their viscosity is highly temperature dependent. The momentum and the energy equations become thus coupled.

To analyse this effect on hydrodynamic and thermal behaviour of the flow, we consider a temperature-dependent consistency [Eq. (8)].

The effect of a temperature-dependent viscosity on the fully developed velocity profiles is shown in Fig. 4. We note a distortion of the profiles, compared to the case of a constant viscosity ($K^*(\theta) = 1$). Actually, the heating of the wall fluid layers causes a wall lubrication of the adjacent fluid layers. As a result, a contraction of the velocity profile takes place to conserve the flow rate. In addition, the increase of the temperature coefficient a^* leads to an increase in the extent of the unyielded region (plug flow region) since the shear stress at the wall decreases due to an increase in the wall velocity. A similar behaviour has been observed by Nouar et al. [22].

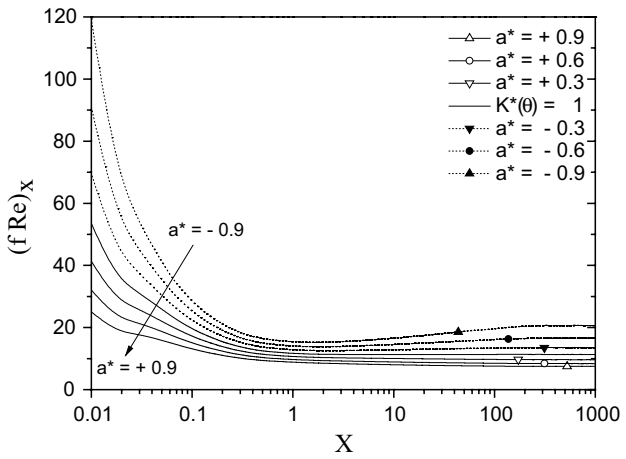

Fig. 6 Axial evolution of the friction factor of Fanning for various values of the dimensionless temperature coefficient. $Re = 20$, $Pr = 50$, $HB = 2$, $Br = 0$

The same behaviour is observed in Fig. 5 which shows the axial evolution of the centreline velocities. The latter increase gradually from the inlet until they attain the fully developed flow.

Table 3 Deviation of the average friction factor of Fanning by considering various values of the dimensionless temperature coefficient

$\lvert a* \rvert$	$\left[\frac{\lvert (f\,Re)_{av,a*} - (f\,Re)_{av,K^*(\theta)=1} \rvert}{(f\,Re)_{av,K^*(\theta)=1}} 100\right](\%)$	
	Heating case ($a^* > 0$)	Cooling case ($a^* < 0$)
0.3	14.58	19.56
0.6	25.60	45.50
0.9	33.55	79.97
1.2	40.23	–
1.5	45.01	–
1.8	48.91	–

$Pr = 50$, $Re = 20$, $HB = 2$, $Br = 0$

Table 4 Deviation of the average Nusselt number by considering various values of the dimensionless temperature coefficient

$\lvert a* \rvert$	$\left[\frac{\lvert Nu_{av,a*} - Nu_{av,K^*(\theta)=1} \rvert}{Nu_{av,K^*(\theta)=1}} 100\right](\%)$	
	Heating case ($a^* > 0$)	Cooling case ($a^* < 0$)
0.3	04.78	00.00
0.6	06.29	00.00
0.9	09.23	04.46
1.2	14.01	–
1.5	14.01	–
1.8	14.01	–

$Pr = 50$, $Re = 20$, $HB = 2$, $Br = 0$

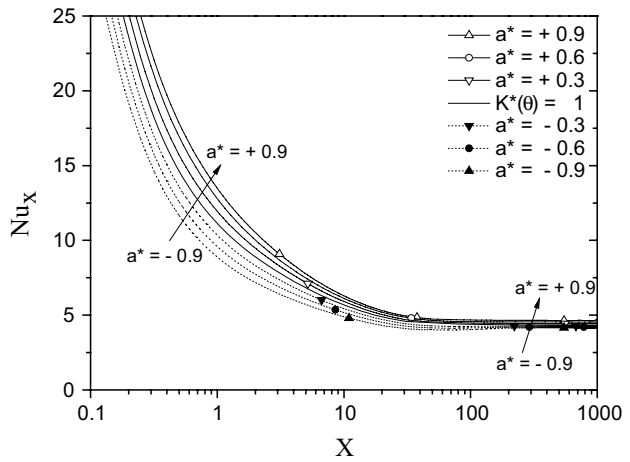

Fig. 7 Axial evolution of the local Nusselt number for various values of the dimensionless temperature coefficient. $Re = 20$, $Pr = 50$, $HB = 2$, $Br = 0$

We notice that the increase of the coefficient a^* leads to the decrease of the centreline velocity. A similar behaviour has been observed by Métivier and Nouar [23] when they consider the Herschel–Bulkley thermodependent flow in a horizontal plane channel. It is to be noted also that the greater values of the centreline velocity are observed in the case of a constant viscosity ($K^*(\theta) = 1$).

Since the viscosity's variation according to the temperature causes important effects on the development of axial velocity profiles, this is directly reflected on the evolution of both the friction factor of Fanning and the Nusselt number.

Figure 6 shows the axial evolution of the friction factor of Fanning according to the dimensionless temperature coefficient's variations. It is worth noting, from this figure, that the increase of the dimensionless temperature coefficient leads to the decrease of the friction factor of Fanning despite the fact that the wall velocity gradient increases (Fig. 4). This can be explained by the fact that the wall effective viscosity decreases according to the expression:

$$(f\,Re)_X = 2\left(\eta_{\text{eff}}\dot{\gamma}^*\right)_{R=0.5} \tag{18}$$

Thus, the increase of the wall velocity gradient is less important than the decrease of the wall effective viscosity, which imposes its variation on the friction factor of Fanning ($f\,Re$) which decreases consequently.

In addition, taking into account the temperature dependency of the fluid's viscosity leads to significant contrasts from the case of a constant viscosity. According to Table 3, these contrasts are more important for the great values of the dimensionless temperature coefficient which corresponds to the cooling case.

Figure 7, which illustrates the axial evolution of the Nusselt number along the pipe, shows that the increase of the dimensionless temperature coefficient a^* leads to the increase of the Nusselt number. Indeed, the viscosity close to the wall is reduced when the coefficient a^* increases. As a result, velocity increases in this region, involving an enhancement of heat transfer close to the wall. It is interesting to note also that the effect of the temperature dependency of the viscosity is more pronounced at the inlet; and becomes less important in the fully developed region.

Hence, neglecting the temperature dependency of the viscosity would underestimate heat transfer about the values shown in Table 4, in terms of average Nusselt number. These values are more significant for the heating case and when increasing the value of the dimensionless temperature coefficient.

It is to be noted that for numerical problems, we were unable to present the cases corresponding to $a^* = -1.2$, -1.5 and -1.8.

3.3 Viscous dissipation for a temperature-dependent Herschel–Bulkley fluid

Viscous dissipation is an energy source, represented by the Brinkman number [in Eq. (4)]. This dimensionless number

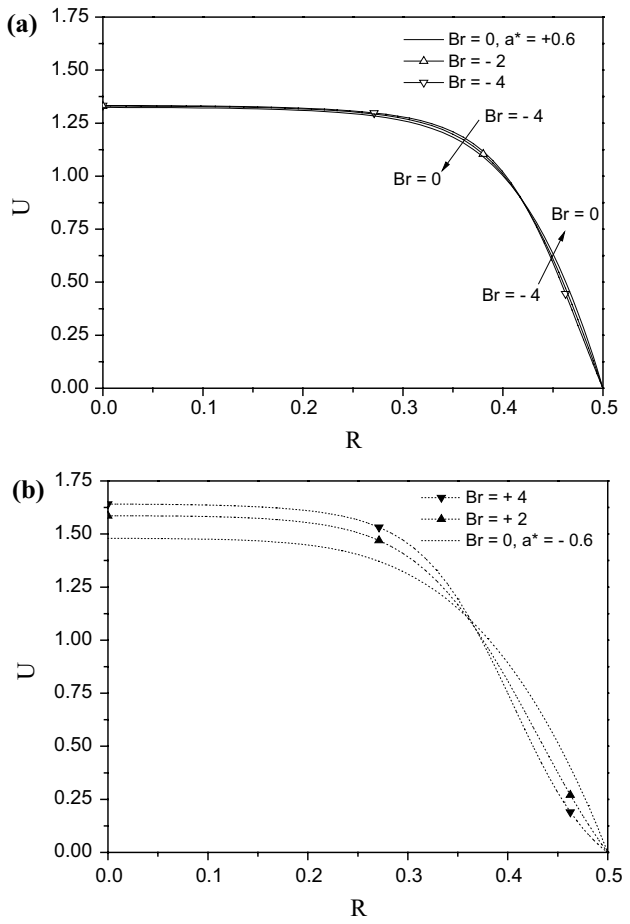

Fig. 8 Fully developed velocity profiles for various values of the Brinkman number. $Re = 20$, $Pr = 50$, $HB = 2$. **a** $a^* = +0.6$, **b** $a^* = -0.6$

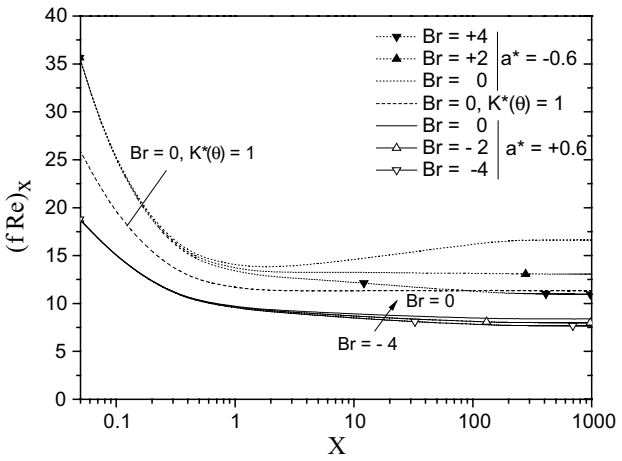

Fig. 9 Axial evolution of the friction factor of Fanning for various values of the Brinkman number. $Re = 20$, $Pr = 50$, $HB = 2$, $a^* = \pm 0.6$

compares the dissipation term with the conduction term in the energy equation. A negative value of the Brinkman number ($Br < 0$) refers that the fluid is wall heated (heating case) while a positive value ($Br > 0$) indicates that the fluid is cooled down (cooling case).

When dealing with non-viscous Newtonian fluids and some non-Newtonian fluids, viscous dissipation is most of the time neglected. However, this is not valid if the fluid is very viscous or viscoplastic, as found in references [2, 3].

On the other hand, when both viscosity temperature dependency and viscous dissipation are considered, the governing equations become strongly coupled. In this case, some authors use the Nahme number instead of the Brinkman number to characterize how much viscous dissipation affects the temperature-dependent viscosity [24, 25]. This choice depends on the temperature characteristic scale. Indeed, for these authors, the temperature is non-dimensionalized against the heat flux. However, in our case, the temperature is non-dimensionalized against the temperature difference ($T_0 - T_w$). Consequently, the effect of viscous dissipation for a temperature-dependent fluid is analysed, in the present study, through the Brinkman number's variations.

It is worth nothing that when viscous dissipation is neglected ($Br = 0$), the fluid undergoes only a wall heating or a wall cooling. However, when taking into account viscous dissipation, the fluid velocity near the wall decreases, in the case of cooling, comparing to the case $Br = 0$. Consequently, the fully wall velocity gradient decreases, as shown in Fig. 8. This can be explained by the fact that when viscous dissipation is introduced for the cooling case, it intensifies the cooling of the fluid near the wall, mainly when the Brinkman number increases. As a result, the fluid is cooled down at the vicinity of the wall and its velocity decreases since the fluid effective viscosity increases. A similar behaviour is observed for the heating case but the effect of the Brinkman number is less noticeable in this case. We can observe also that the wall velocity gradient is more important in the heating case.

The effect of both viscous dissipation and viscosity temperature dependency on the axial evolution of the friction factor of Fanning is illustrated in Fig. 9. As it can be seen, all the curves depict a continuous decrease from the inlet till the outlet of the pipe where $(f\,Re)_x$ reaches asymptotic values corresponding to the fully developed flow. However, only the curve corresponding to the case of cooling without viscous dissipation ($Br = 0$ and $a^* = -0.6$) depicts a different behaviour. Indeed, the latter from a section from the inlet ($X = 1.22$) shows a weak increase before reaching asymptotic values. It is interesting to note that the curves corresponding to the cooling case ($a^* = -0.6$ and $Br > 0$) are located above the ones corresponding to a constant viscosity without viscous dissipation ($K^*(\theta) = 1$ and $Br = 0$), providing thus the greatest values of the friction factor of Fanning. On the other hand, the heating case ($a^* = +0.6$ and $Br < 0$) offers

Table 5 Deviation of the average friction factor of Fanning for a temperature-dependent fluid when taking into account viscous dissipation

a^*	Br	$\left[\frac{\lvert(f\,Re)_{av,a*,Br}-(f\,Re)_{av,K^*(\theta)=1,Br=0}\rvert}{(f\,Re)_{av,K^*(\theta)=1,Br=0}}100\right](\%)$
+0.6	−2	28.96
	−4	31.76
−0.6	+2	15.91
	+4	33.21

$Pr = 50$, $Re = 20$, $HB = 2$, $a^* = \pm 0.6$

Table 6 Deviation of the Nusselt number for a temperature-dependent fluid when considering viscous dissipation

	a^*	Br	$\left[\frac{\lvert Nu_{a*,Br}-Nu_{K^*(\theta)=1,Br=0}\rvert}{Nu_{K^*(\theta)=1,Br=0}}100\right](\%)$
Nu_{asy}	+0.6	−2	314.66
		−4	318.80
Nu_{av}	−0.6	+2	168.30
		+4	150.99

$Pr = 50$, $Re = 20$, $HB = 2$, $a^* = \pm 0.6$

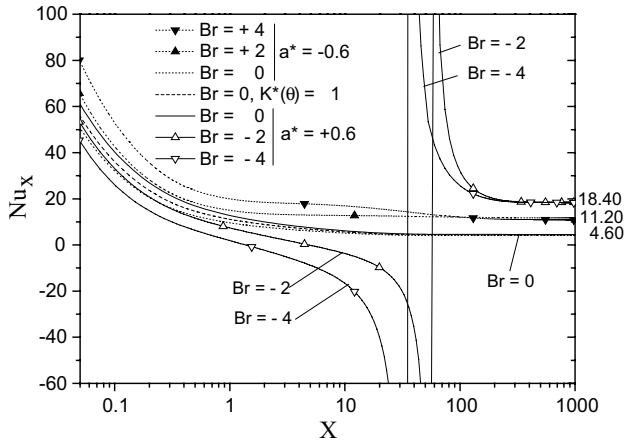

Fig. 10 Axial evolution of the local Nusselt number for various values of the Brinkman number. $Re = 20$, $Pr = 50$, $HB = 2$, $a^* = \pm 0.6$

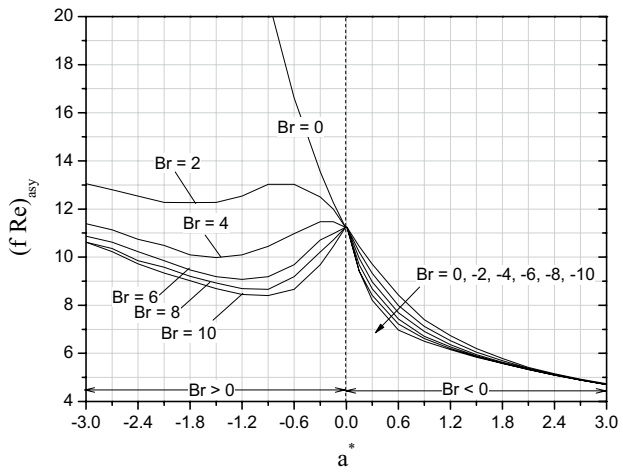

Fig. 11 Asymptotic values of the friction factor of Fanning according to the dimensionless temperature coefficient and the Brinkman number. $Pr = 50$, $Re = 20$, $HB = 2$, $n = 0.5$

the weakest values of the friction factor of Fanning despite the fact that the wall velocity gradient values are greater than the one corresponding to the cooling case (Fig. 8). The values of the friction factor of Fanning are especially weaker as the Brinkman number increases (in absolute value).

Industrial equipment design requires the knowledge of pressure drop. The latter is closely related to both wall velocity gradient and the fluid viscosity and thus, to the friction factor of Fanning. So and from the presented figures, neglecting viscous dissipation or the viscosity temperature dependency could lead to significant errors in the design when dealing with very viscous fluids such as viscoplastic ones. Table 5 shows the deviations of the average friction factor of Fanning along the pipe, from the constant viscosity case without viscous dissipation. It can be seen that these gaps are more important than that obtained in the case of a temperature-dependent fluid without viscous dissipation (Table 3). On the other hand, the increase of the Brinkman number (in absolute value) leads to significant deviations compared to the case when both temperature dependency and viscous dissipation are neglected.

Regarding heat transfer characteristics within the pipe when viscous dissipation is taken into account for a temperature-dependent fluid, Fig. 10 illustrates the axial evolution of the local Nusselt number. A pronounced decrease of the latter is observed near the inlet, followed by a tendency to asymptotic values independent of the Brinkman number, corresponding to the thermal fully developed flow, according to whether it is a cooling or a heating case. These values are equals to 18.40 and 11.20 for heating ($a^* = +0.6$ and $Br < 0$) and cooling ($a^* = -0.6$ and $Br > 0$) cases, respectively.

The results are different of those obtained in the case of a temperature-dependent viscosity when neglecting viscous dissipation (Fig. 7), for which there was almost no effect of the dimensionless temperature coefficient in the fully developed region. The asymptotic value of the Nusselt number approaches that obtained for the case of a constant viscosity when viscous dissipation is neglected ($K^*(\theta) = 1$ and $Br = 0$). It is also interesting to note, on the other hand, that in the heating case ($Br < 0$), the curves present a discontinuity. Moreover, due to the change in heat direction [14, 26], negative values of the Nusselt number appear.

It is worth noting that heat transfer is more significant in the thermal fully developed region, when the Brinkman number increases for both heating and cooling cases.

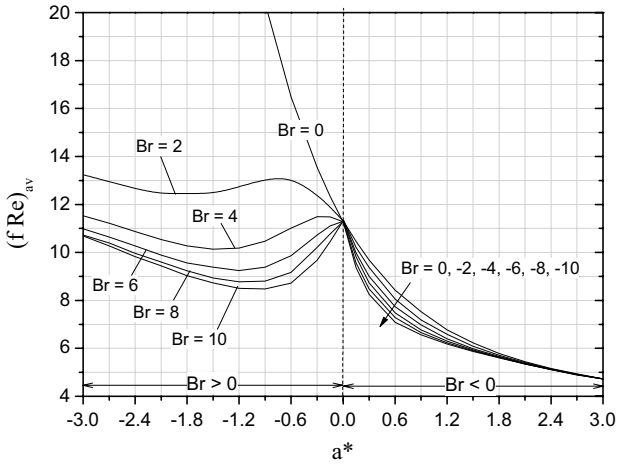

Fig. 12 Average values of the friction factor of Fanning according to the dimensionless temperature coefficient and the Brinkman number. $Pr = 50$, $Re = 20$, $HB = 2$, $n = 0.5$

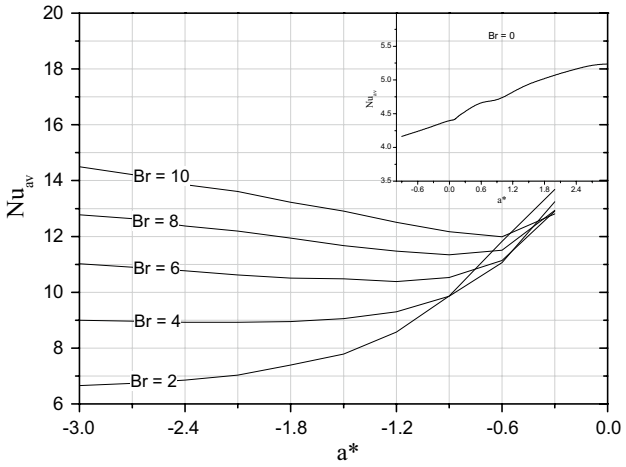

Fig. 14 Average values of the Nusselt number according to the dimensionless temperature coefficient and the Brinkman number. $Pr = 50$, $Re = 20$, $HB = 2$, $n = 0.5$

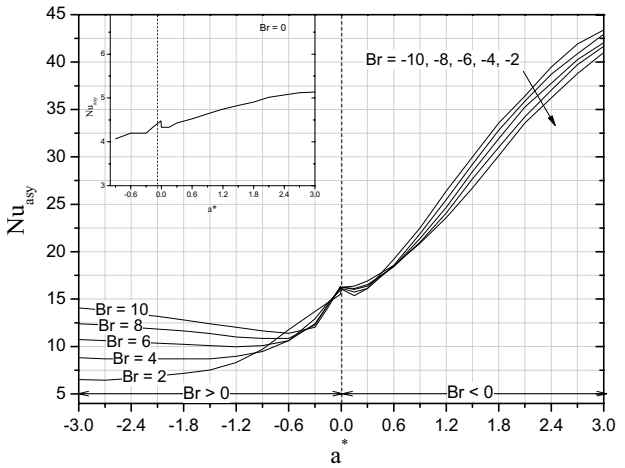

Fig. 13 Asymptotic values of the Nusselt number according to the dimensionless temperature coefficient and the Brinkman number. $Pr = 50$, $Re = 20$, $HB = 2$, $n = 0.5$

This is more noticeable in the heating case ($a^* = +0.6$ and $Br < 0$). It is also interesting to note that the effect of the temperature-dependent viscosity is more noteworthy when viscous dissipation is taken into account.

Thus, neglecting both viscous dissipation and the temperature dependency of the fluid's viscosity leads to underestimate heat transfer causing consequently, errors in the equipment design. This is noticeable in Table 6 where it can be seen that heat transfer is underestimated of about 300 % when both viscous dissipation and thermodependency of the fluid's viscosity are neglected. It is important to note that these deviations are calculated in relation to the mean values of the Nusselt number in the wall cooling case ($a^* = -0.6$ and $Br > 0$) and to the asymptotic values of the Nusselt number in the wall heating case ($a^* = +0.6$ and $Br < 0$), because of the negative values of the Nusselt number and discontinuities observed in curves. Furthermore, these deviations are more important in comparison to the case when only the temperature dependency of the viscosity is taken into account.

3.4 Abacuses

To sum up the results obtained in the present study, abacuses depicting the friction factor of Fanning and the Nusselt number variations according to both Brinkman number and the dimensionless temperature coefficient are plotted in Figs. 11, 12, 13 and 14. These abacuses can be useful to predict pressure drop and heat transfer for the steady flow of a temperature-dependent shear-thinning Herschel–Bulkley, for which the flow index is equal to 0.5, within a circular pipe maintained at a uniform wall temperature, when viscous dissipation is taken into account.

We can observe, from these figures, various behaviours of the asymptotic and average values of both the friction factor of Fanning and the Nusselt number according to whether the absolute value of the dimensionless temperature coefficient is less or greater than the value considered previously (i.e. 0.6).

4 Conclusion

A numerical study, based on the finite volume method, was investigated to analyse the hydrodynamic and thermal properties of an incompressible shear-thinning Herschel–Bulkley fluid flow. The flow, which is the seat of a forced convection heat transfer, is steady and laminar and takes place within a pipe of a circular cross section with a uniform wall

temperature. The study was mainly focused on the effect of both viscous dissipation and the temperature dependency of the fluid's consistency on the flow characteristics and abacuses were proposed at the end of the work.

The results show that taking into account the temperature dependency of the fluid's consistency involves modifications on the flow structure compared to the case of a constant consistency. These modifications are more noticeable on hydrodynamic properties given that neglecting the viscosity's temperature dependency leads to undervalue the average friction factor of Fanning, especially in the cooling case. This underestimation is about 80 % for $a^* = -0.9$. However, heat transfer is underestimate of only about 14 % for $a^* = +1.8$.

On the other hand, this underestimation becomes more significant when viscous dissipation is taken into account. Indeed, besides the whole modification observed on the Nusselt number's curves, which are characterized in the case of heating ($Br < 0$), by the existence of discontinuities and negatives values, viscous dissipation affects also hydrodynamic properties since when the viscosity varies according to the temperature, the governing equations become coupled and the temperature dependency of the viscosity intensifies the modifications observed on both hydrodynamic and thermal characteristics.

Furthermore, neglecting both viscous dissipation and the temperature dependency of the fluid's viscosity concerns principally heat transfer since the underestimation reaches more than 300 % in the heating case.

Finally, to sum up our results, abacuses depicting the friction factor of Fanning and the Nusselt number variations according to both the Brinkman number and the dimensionless temperature coefficient were plotted. These abacuses can be useful to predict pressure drop and heat transfer of a shear-thinning Herschel–Bulkley fluid, of a flow index close to 0.50, flow inside pipes subjected to a uniform wall temperature, by taking a Peclet and a Herschel–Bulkley numbers equal, respectively, to 1000 and 2.

References

1. Hammad KJ, Vradis GC (1996) Viscous dissipation and heat transfer in pulsatile flows of a yield stress fluid. Int Commun Heat Mass Transf 23–5:599–612
2. Vradis GC, Dougher J, Kumar S (1993) Entrance pipe flow and heat transfer for a Bingham plastic. Int J Heat Mass Transf 36–3:543–552
3. Min T, Choi HG, Yoo JY, Choi H (1997) Laminar convective heat transfer of a Bingham plastic in a circular pipe II. Numerical approach hydrodynamically developing flow and simultaneously developing flow. Int J Heat Mass Transf 40–15:3689–3701
4. Nascimento UCS, Macêdo EN, Quaresma JNN (2002) Thermal entry region analysis through the finite integral transform technique in laminar flow of Bingham fluids within concentric annular ducts. Int J Heat Mass Transf 45:923–929
5. Soares EJ, Naccache MF, Souza Mendes PR (2003) Heat transfer to viscoplastic materials flowing axially through concentric annuli. Int J Heat Fluid Flow 24:762–773
6. Khatyr R, Ouldhadda D, Il Idrissi A (2002) Approche analytique de la convection forcée des fluides de Bingham dans un tube. C R Méc 330:69–75
7. Khatyr R, Ouldhadda D, Il Idrissi A (2003) Viscous dissipation effects on the asymptotic behaviour of laminar forced convection for Bingham plastics in circular ducts. Int J Heat Mass Transf 46:589–598
8. Piau JM (2007) Carbopol gels: elastoviscoplastic and slippery glasses made of individual swollen sponges Meso- and macroscopic properties, constitutive equations and scaling laws. J Nonnewton Fluid Mech 144:1–29
9. Duvaut G, Lions JL (1972) Transfert de chaleur dans un fluide de Bingham dont la viscosité dépend de la température. J Funct Anal 11:93–110
10. Vinay G, Wachs A, Agassant JF (2005) Numerical simulation of non-isothermal viscoplastic waxy crude oil flows. J Nonnewton Fluid Mech 128:144–162
11. Soares M, Naccache MF, Souza Mendes PR (1999) Heat transfer to viscoplastic materials flowing laminarly in the entrance region of tubes. Int J Heat Fluid Flow 20:60–67
12. Nouar C (2005) Thermal convection for a thermo-dependent yield stress fluid in an axisymmetric horizontal duct. Int J Heat Mass Transf 48:5520–5535
13. Peixinho J, Desaubry C, Lebouche M (2008) Heat transfer of a non-Newtonian fluid (Carbopol aqueous solution) in transitional pipe flow. Int J Heat Mass Transf 51:198–209
14. Labsi N, Benkahla YK, Boutra A, Ammouri A (2013) Heat and flow properties of a temperature dependent viscoplastic fluid including viscous dissipation. J Food Process Eng 36:450–461
15. Mitsoulis E (2004) On creeping drag flow of a viscoplastic fluid past a circular cylinder: wall effects. Chem Eng Sci 59:789–800
16. Papanastasiou TC (1987) Flow of materials with yield. J Rheol 31:385–404
17. Mitsoulis E, Galazoulas S (2009) Simulation of viscoplastic flow past cylinders in tubes. J Nonnewton Fluid Mech 158:132–141
18. Patankar SV (1980) Numerical heat transfer and fluid flow. Hemisphere Publishing Co., New York
19. Peixinho J, Nouar C, Desaubry C, Théron B (2005) Laminar transitional and turbulent flow of yield stress fluid in a pipe. J Nonnewton Fluid Mech 128:172–184
20. Jambal O, Shigechi T, Davaa G, Momoki S (2005) Effects of viscous dissipation and fluid axial heat conduction on heat transfer for non-Newtonian fluids in ducts with uniform wall temperature, part I: parallel plates and circular ducts. Int Commun Heat Mass Transf 32:1165–1173
21. Quaresma JNN, Macêdo EN (1998) Integral transform solution for the forced convection of Herschel–Bulkley fluids in circular tubes and parallel-plates ducts. Braz J Chem Eng. doi:10.1590/S0104-66321998000100008
22. Nouar C, Devienne R, Lebouché M (1994) Convection thermique pour un fluide de Herschel–Bulkley dans la région d'entrée d'une conduite. Int J Heat Mass Transf 37–1:1–12
23. Métivier C, Nouar C (2009) Linear stability of the Rayleigh–Bénard Poiseuille flow for thermodependent viscoplastic fluids. J Nonnewton Fluid Mech 163:1–8
24. Winter HH (1977) Viscous dissipation in shear flows of molten polymers. Adv Heat Transf 13:205–267
25. Mitsoulis E, Abdali SS, Markatos NC (1993) Flow simulation of Herschel–Bulkley fluids through extrusion dies. Can J Chem Eng 71:147–160
26. Aydin O (2005) Effects of viscous dissipation on the heat transfer in forced pipe flow. Part 1: both hydrodynamically and thermally fully developed flow. Energy Convers Manag 46:757–769